Nanoscale Research Letters

NANO EXPRESS Open Access

Controllable Two-dimensional Perovskite Crystallization via Water Additive for High-performance Solar Cells

Ziji Liu[1†], Hualin Zheng[1†], Detao Liu[1], Zhiqing Liang[1*], Wenyao Yang[2], Hao Chen[1], Long Ji[1], Shihao Yuan[1], Yiding Gu[1] and Shibin Li[1*]

Abstract

Steering the crystallization of two-dimensional (2D) perovskite film is an important strategy to improve the power conversion efficiency (PCE) of 2D perovskite solar cells (PVSCs). In this paper, the deionized water (H_2O) additive is introduced into the perovskite precursor solution to prepare high-quality 2D perovskite films. The 2D perovskite film treated with 3% H_2O shows a good surface morphology, increased crystal size, enhanced crystallinity, preferred orientation, and low defect density. The fabricated 2D PVSC with 3% H_2O exhibits a higher PCE compared with that without H_2O (12.15% vs 2.29%). Furthermore, the shelf stability of unsealed devices with 3% H_2O under ambient environment is significantly improved. This work provides a simple method to prepare high-quality 2D perovskite films for efficient and stable 2D PVSCs.

Keywords: Two-dimensional perovskite, Crystallization, Additive, Water, Solar cell

Introduction

Recently, two-dimensional (2D) layered perovskites have drawn extensive attention due to their enhanced moisture resistance versus their 3D counterparts, such as $CH_3NH_3PbI_3$ ($MAPbI_3$) and $HC(NH_2)_2PbI_3$ ($FAPbI_3$). The 2D perovskite with the formula of $A_2B_{n-1}M_nX_{3n+1}$ (Ruddlesden–Popper phase), where B is MA^+, FA^+, or Cs^+, M is Pb^{2+} or Sn^{2+}, X stands for halide anion, n refers to the number of planes of the corner-sharing $[MX_6]^{4-}$ octahedral, can be formed by incorporating organic long-chain ligands A (such as phenethylammonium (PEA^+) or butylammonium (BA^+)) in the inorganic framework. These 2D perovskites possess many unique optoelectronic properties, and have been developed for use in both solar cells [1, 2] and light-emitting diodes [3]. However, the exciton binding energy of the layered 2D perovskite is enhanced on account of the dielectric confinement effect between the organic layer and the inorganic framework [4], which substantially limits the exciton dissociation in the electrical field [5]. Meanwhile, the bulky organic ligands would form insulating spacing layers and inhibit charge transport between neighboring inorganic slabs. Thus, the PCE of 2D PVSCs is much lower than that of their 3D counterparts, which has been already above 25% [6].

To obtain high-performance 2D PVSCs, many efforts have been made, including the hot-coasting [7], additive engineering [8–14], composition engineering [15–26], precursor solvent engineering [27–30], interfacial engineering [31–35], and other special treatments [13, 36, 37]. Among these methods, additive engineering is the frequently used method due to its simplicity and effectiveness. Zhang et al. found that the vertically oriented 2D layered perovskite film can be deposited via incorporating ammonium thiocyanate (NH_4SCN) additive into the perovskite precursor solution [8, 9]. Therefore, the PCE of 2D PVSCs drastically increases from 0.56 to 11.01%.

* Correspondence: liangzq@uestc.edu.cn; shibinli@uestc.edu.cn
†Ziji Liu and Hualin Zheng contributed equally to this work.
[1]State Key Laboratory of Electronic Thin Films and Integrated Devices, and School of Optoelectronic Science and Engineering, University of Electronic Science and Technology of China (UESTC), Chengdu 610054, Sichuan, China
Full list of author information is available at the end of the article

Qing et al. demonstrated that the quality of 2D perovskite film can be improved by a synergistic effect of two additives in the perovskite precursor solution [10]. Consequently, a hysteresis-free 2D PVSCs with a PCE exceeding 12% has been obtained. Yu et al. showed that the film morphology and the charge transportation in perovskites can be effectively controlled through adding both ammonium chloride (NH_4Cl) additive and dimethyl sulfoxide (DMSO) solvent into the precursor solution and a PCE of 13.41% was achieved [11]. Fu et al. reported an efficient 2D PVSCs processed with NH_4SCN and NH_4Cl additives, yielding an optimal PCE of 14.1% [12]. In our previous work, we found that DMSO and thiosemicarbazide (TSC) exhibit a synergistic effect in improving the morphology, crystallization, and orientation of 2D perovskite films [14]. It is speculated that both DMSO and TSC are Lewis bases [38], which regulate the crystallization process of 2D perovskite through coordination with the perovskite precursor components. As a result, the efficient and stable 2D PVSCs with a champion PCE of 14.15% were obtained.

In the Lewis acid–base concept, a water molecule is an oxygen donor Lewis base that can bond with the lead iodide (PbI_2) Lewis acid. Meanwhile, the physical and chemical thermodynamic properties of water molecules, like boiling point, solubility, and vapor pressure, are different from frequently-used N,N-dimethylformamide (DMF) solvent. A series of studies have revealed that the water added into the perovskite precursor solution can control the 3D perovskite crystallization, leading to a better photovoltaic performance [39–44]. However, as we all know, using H_2O as an additive in 2D PVSC has not been reported yet so far.

In this study, water molecules as additive were introduced into perovskite precursor solutions to control the crystallization of 2D perovskite film. The 2D perovskite film ($BA_2MA_3Pb_4I_{13}$, n = 4) treated with a suitable amount of water shows good film morphology, enhanced crystallinity and increased orientation ordering. This high-quality 2D perovskite film contributes to the lower trap-state density and then higher photovoltaic performance of 2D PVSCs. The PCE of 2D PVSCs has been improved from 2.29 to 12.15%. More interestingly, water additive based devices exhibit obviously improved shelf stability.

Method

Materials

Methyl-ammonium iodide (MAI), PbI_2, PEDOT:PSS (4083) aqueous solution, n-butylammonium iodide (BAI), phenyl-C61-butyric acid methyl ester ($PC_{61}BM$), spiro-MeOTAD (2,29,7,79-tetrakis(N,N-di-p-methoxyphenylamine)-9,9-spirobifluorene), 4-tert-butylpyridine, lithium bis (trifluoromethylsulphonyl) imide, and bathocuproine (BCP) were ordered from Xi'an Polymer Light Technology Cory. DMF, chlorobenzene, and acetonitrile were purchased from Sigma-Aldrich. Isopropanol was purchased from You Xuan Tech. All reagents and solvents were used directly without further purification.

Precursor Solution

The pristine $BA_2MA_3Pb_4I_{13}$ precursor solution (0.85 M) was prepared by mixing BAI, MAI, PbI_2 with a molar ratio of 0.5: 0.75: 1 in DMF. The precursors with various amounts of deionized water were prepared by adding different volume ratios of deionized water into the pristine precursor solution.

Device Fabrication

The indium tin oxide (ITO) substrates were ultrasonically washed with detergent, acetone, absolute ethyl alcohol, and deionized water in succession, followed by a 15 min UV-ozone treatment. For the hole collection layers, PEDOT:PSS aqueous solution was spin-coated onto the cleaned ITO substrates at 4000 rpm for 40 s. After the spin-coating, the PEDOT:PSS films were heated in air at 150 °C for 15 min, and then transferred into the glovebox. For the photoelectric conversion layers, the ITO/PEDOT:PSS substrates were preheated at 100 °C for 3 min, followed by spin coating different perovskite precursor solutions at 5000 rpm for 25 s and then annealing at 100 °C for 10 min. For the electron extraction layers, the solution of $PC_{61}BM$ (15 mg/mL in chlorobenzene) was spin-coated onto the perovskite layers at 2000 rpm for 30 s. Next, BCP in isopropanol with a concentration of 0.8 mg/ml was spin-coated at 5000 rpm for 30 s. Finally, 70 nm Ag electrodes were thermally evaporated on the BCP layers through the shadow masks. The effective device area was 0.04 cm^2. For the preparation of hole-only devices, the spiro-OMeTAD layers were deposited onto the 2D perovskite/PEDOT:PSS/ITO substrates by spin-coating spiro-OMeTAD solution at 4000 rpm for 30 s followed by evaporation of 70 nm gold electrode on the top of the device. The spiro-OMeTAD solution was prepared by dissolving 90 mg spiro-OMeTAD, 22 μL of a stock solution of 520 mg/mL lithium bis(trifluoromethylsulphonyl)imide in acetonitrile and 36 μL 4-tert-butylpyridine in 1 mL chlorobenzene.

Measurement and Characterization

The current density-voltage (J-V) curves of PVSCs were measured by Keithley source unit 2400 under AM 1.5G sun intensity illumination by a solar simulator from Newport Corp. The scanning rate of J-V curves is 0.2 V/s. Scanning electron microscope (SEM) measurements were conducted on field emission fitting SEM (FEI-Inspect F50, Holland). The grazing incidence wide-angle X-ray scatting (GIWAXS) measurements were conducted at BL14B1

beamline at Shanghai Synchrotron Radiation Facility, Shanghai, China, with a 0.6887 Å primary beam, 0.2° incident angle. The absorption spectrum of 2D perovskite was measured using Shimadzu 1500 spectrophotometer. External quantum efficiencies were measured by QTEST HIFINITY 5 (Crowntech). Time-resolved photoluminescence spectrum was performed with a Fluo Time 300 (Pico Quant) spectrofluorometer.

Results and Discussion

To investigate the influence of H_2O additive on the performance of 2D PVSCs, we fabricated the inverted devices with the configuration of indium tin oxide (ITO)/PEDOT:PSS/$BA_2MA_3Pb_4I_{13}$/$PC_{61}BM$/BCP/Ag as shown in Fig. 1a. The deionized water was mixed with perovskite precursor solution with a varied volume ratio from 0 to 5%. The photocurrent density–voltage (*J–V*) curves of the champion 2D PVSCs based on perovskite with various amounts of water additive under illumination of AM 1.5G, 100 mW/cm^2 are shown in Fig. 1b, and the corresponding photovoltaic parameters are listed in Table 1. The control device without water additive exhibits a low open-circuit voltage (V_{oc}) of 0.84 V, a short-circuit current density (J_{sc}) of 5.73 mA/cm^2, a fill factor (*FF*) of 47.63 %, resulting in a poor *PCE* of 2.29 %. From Table 1, it is clear that the suitable amount of H_2O additive improves the corresponding photovoltaic performance of the devices dramatically. In the case of 2D perovskite with 3% H_2O, the best-performing device shows a *PCE* of 12.15 %, with a V_{oc} of 1.06 V, J_{sc} of 15.80 mA/cm^2, and *FF* of 72.56 %. The significant improvement in PCE is attributed to the additive-treated perovskite film, which shows a higher crystallinity, larger brick-like grains, uniform morphology, and vertical-orientation perpendicular to the substrate. The details will be discussed below. By further increasing the volume ratio of H_2O to 5%, the photovoltaic parameters of PVSCs were deteriorated. Figure 1c presents the steady-state photocurrent density where PCE is a function of time at the maximum power point (0.84 V). The PCE of the champion device with 3% H_2O stabilizes at 11.78% (black) with a photocurrent density of 14.02 mA/cm^2 (red) in

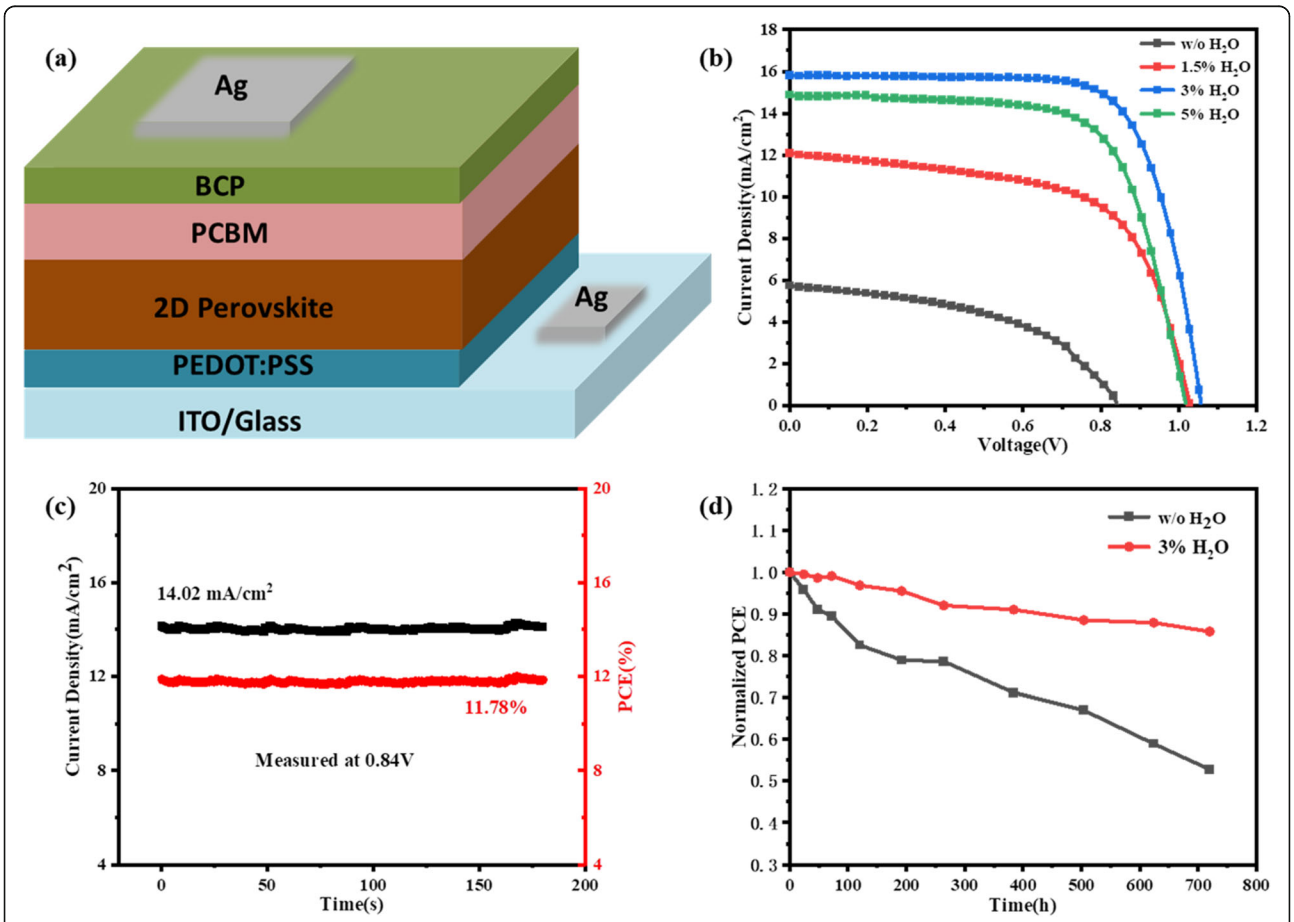

Fig. 1 **a** Schematic illustration of PVSC structure. **b** J-V curves of PVSCs based on $BA_2MA_3Pb_4I_{13}$ films deposited from perovskite precursor solutions doped with different volume H_2O. **c** Steady-state photocurrent and PCE of the champion device 1 sun condition. **d** Long-term stability of the unsealed device without and with 3% H_2O

Table 1 The photovoltaic parameters of the champion PVSCs based on perovskite precursor solution with and without water additive

Doping ratio	V_{oc} (V)	J_{sc} (mA/cm^2)	*FF* (%)	PCE_{max} (%)	PCE_{avg} (%)
w/o H_2O	0.84	5.73	47.63	2.29	1.85
1.5% H_2O	1.03	12.07	61.40	7.63	6.59
3% H_2O	1.06	15.80	72.56	12.15	11.38
5% H_2O	1.02	14.88	68.38	10.38	9.02

the scan time of 200 s, and it is close to the value extracted from *J-V* curve. Importantly, the shelf stability is one of the key requirements for practical application of PVSCs. Both the unsealed devices without and with 3% H_2O were stored in air atmosphere with relative humidity of 25 ± 5% at 25 °C to examined evolution of their PCE as a function of time. As shown in Fig. 1d, the device with 3% H_2O still retained 85.76 % of its initial PCE after 720 h, which was much stable than that of the device without H_2O (52.76 %). The significantly improved stability is attributed to the stable hydrated 2D perovskites that may be generated during the spin-coating and annealing process. The stable hydrated 2D perovskites resist the decomposition of 2D perovskite film to some extent [39, 40]. On the basis of above results, we conclude that the device treated with optimal water content not only yields superior photovoltaic performance but also shows a good stability.

The statistical data for photovoltaic parameters of 16 PVSCs in each case are shown in Fig. 2a–d. The devices without and with 1.5%, 3%, and 5% H_2O present the best PCE of 2.29%, 7.63%, 12.15%, and 10.38% with the average value of 1.85%, 6.59%, 11.38%, and 9.02%, respectively (Table 1). These statistical data show the same tends as their corresponding champion devices, proving the statistically meaningful performance improvements of the device upon a suitable amount of deionized water.

The SEM was conducted to evaluate the effects of H_2O additive on morphology and coverage of 2D perovskite films. The top-view SEM images of $BA_2MA_3Pb_4I_{13}$ film with various amounts of H_2O additive are shown in Fig. 3a-c, and the corresponding cross-section SEM images are

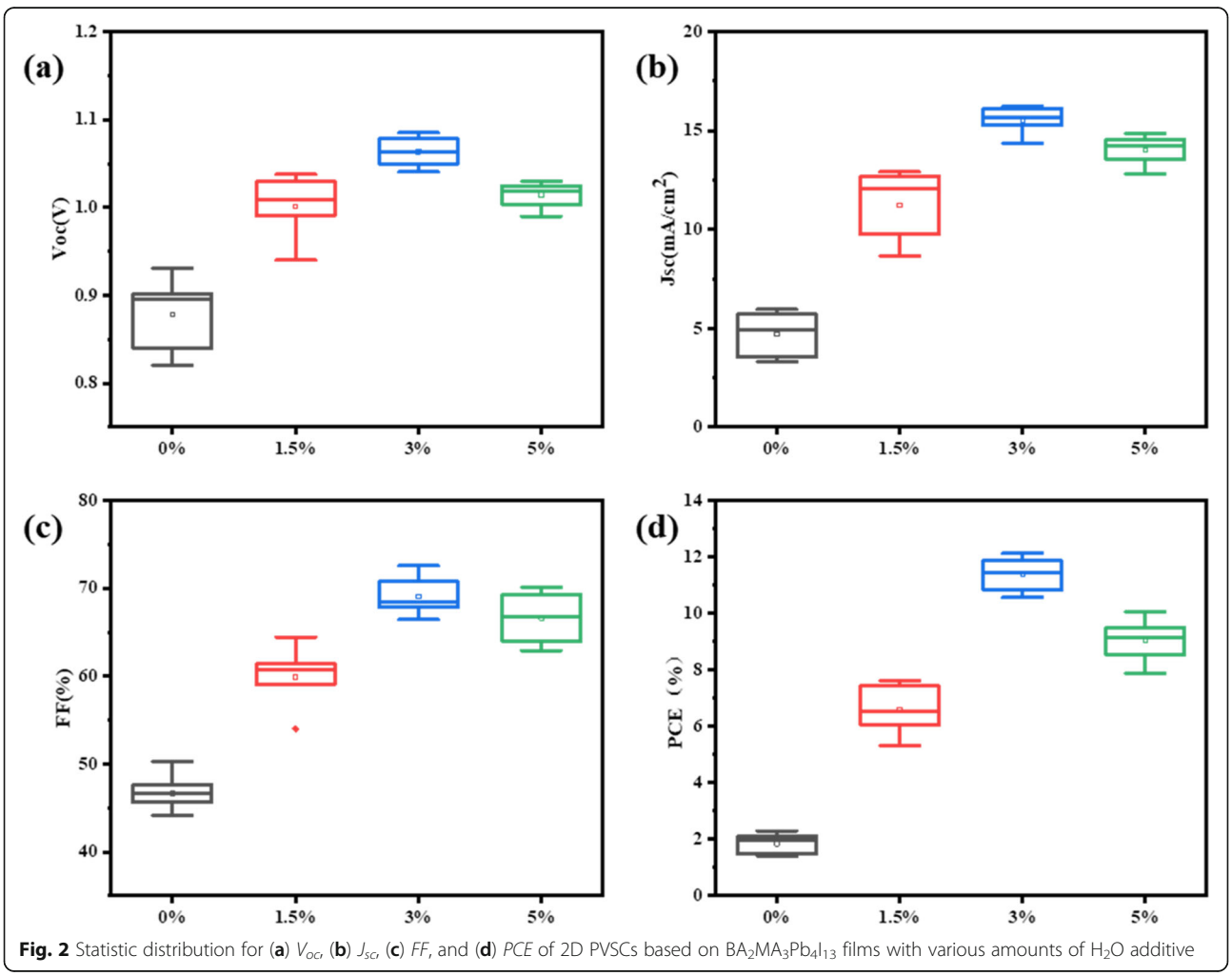

Fig. 2 Statistic distribution for (**a**) V_{oc}, (**b**) J_{sc}, (**c**) *FF*, and (**d**) *PCE* of 2D PVSCs based on $BA_2MA_3Pb_4I_{13}$ films with various amounts of H_2O additive

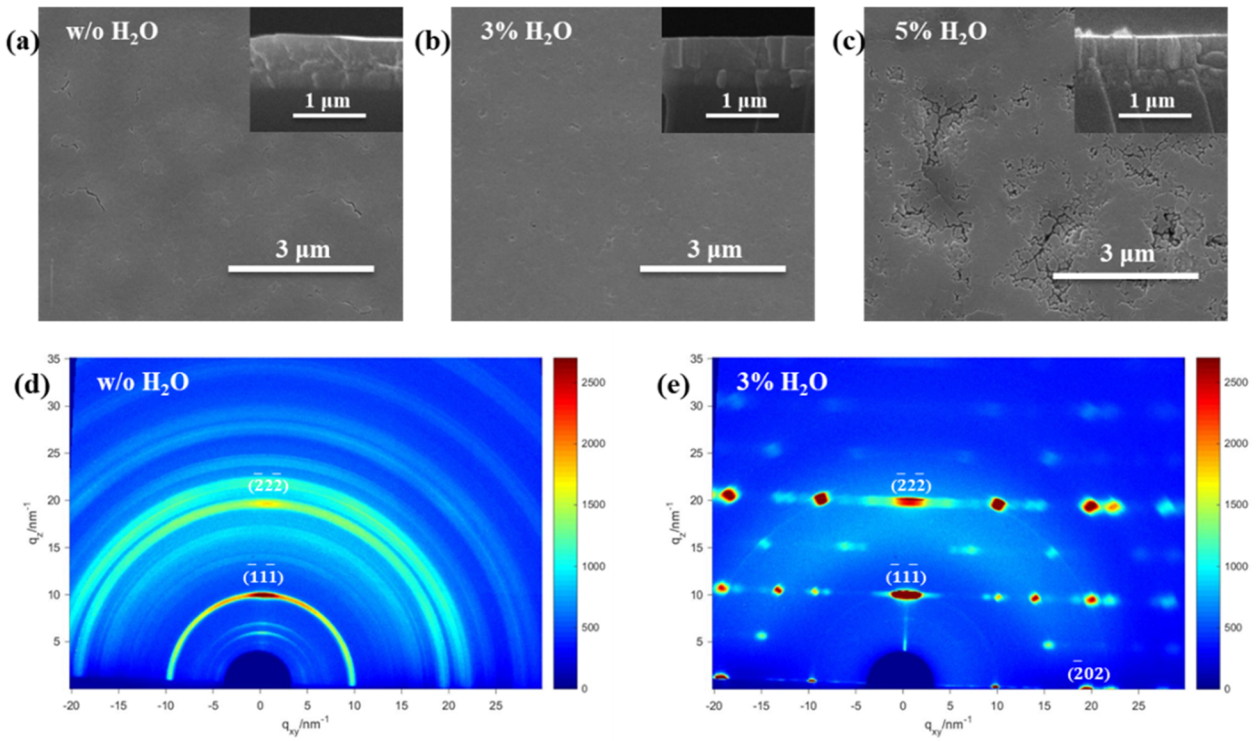

Fig. 3 a-c Top-view SEM images and cross-section SEM images (insets) of $BA_2MA_3Pb_4I_{13}$ films with various amounts of H_2O additive. GIWAXS patterns of $BA_2MA_3Pb_4I_{13}$ film: (**d**) without H_2O additive and (**e**) with 3% H_2O additive

shown in the insets of Fig. 3a-c. The perovskite film without H_2O (denoted as perovskite-w/o H_2O) exhibits a poor morphology with small amounts of cracks and pinholes, while the film with 3% H_2O (denoted as perovskite-3% H_2O) shows a more uniform surface without cracks. A large amount of voids and cracks can be observed when 5% H_2O (denoted as perovskite-5% H_2O) was added, which is mainly due to the decomposition of the hydrate perovskite caused by excessive bulk H_2O [41]. Besides, as shown in the inset of Fig. 3a, the film without H_2O additive is constructed of random-oriented small crystalline grains with lots of grain boundaries. The grain size of the perovskite-3%H_2O film is larger than that of the perovskite-5% H_2O film, though they both exhibit a vertically oriented brick-like morphology. The larger grains in 2D perovskite film results in almost no grain boundary along the vertical direction. It has been reported that grain boundaries are regions where the trap states are mainly distributed [45, 46]. Therefore, the perovskite-3% H_2O films with larger vertically oriented crystal grains contribute to efficient PVSCs.

The GIWAXS patterns have been used to identify the role of water additive in the crystal growth of 2D perovskite films further. We speculate that water additive can regulate the crystallization process of perovskite because of its lower boiling point and higher vapor pressure compared with DMF [40]. Furthermore, incorporating a suitable amount of water into DMF increases the solubility of perovskite ionic compound, leading to the improved quality of the perovskite films with enhanced crystallinity [47]. The SEM and GIWAXS results in this work are consistent with the speculation. As shown in Fig. 3d, the perovskite-w/o H_2O film displays several Bragg rings at specific q values, indicating mainly random oriented crystal grains within this polycrystalline film. However, the perovskite-3% H_2O film shows sharp and discrete Bragg spots along the same q position (Fig. 3e), which suggests the well-aligned crystal grains with (111) planes parallel to the substrate [17]. Moreover, the darker Bragg spots are observed in perovskite-3% H_2O film whereas the less apparent diffraction rings in perovskite-w/o H_2O film, which demonstrates the increased crystallinity of perovskite-3% H_2O film. The highly oriented perovskite-3% H_2O film that is perpendicular to the substrate can form an efficient carrier transport channel, leading to improved photovoltaic performance [14, 17].

To reveal the impact of morphological and crystallographic changes resulted from the addition of water on the optical properties of films, we carried out absorption spectroscopy measurement, as shown in Fig. 4a. Both the perovskite-w/o H_2O film and the perovskite-3% H_2O film exhibit multiple exciton absorption peaks in the UV-Vis absorption spectra, indicating the existence of multiple perovskite phases with different n values, although nominally prepared as "n = 4". However, the

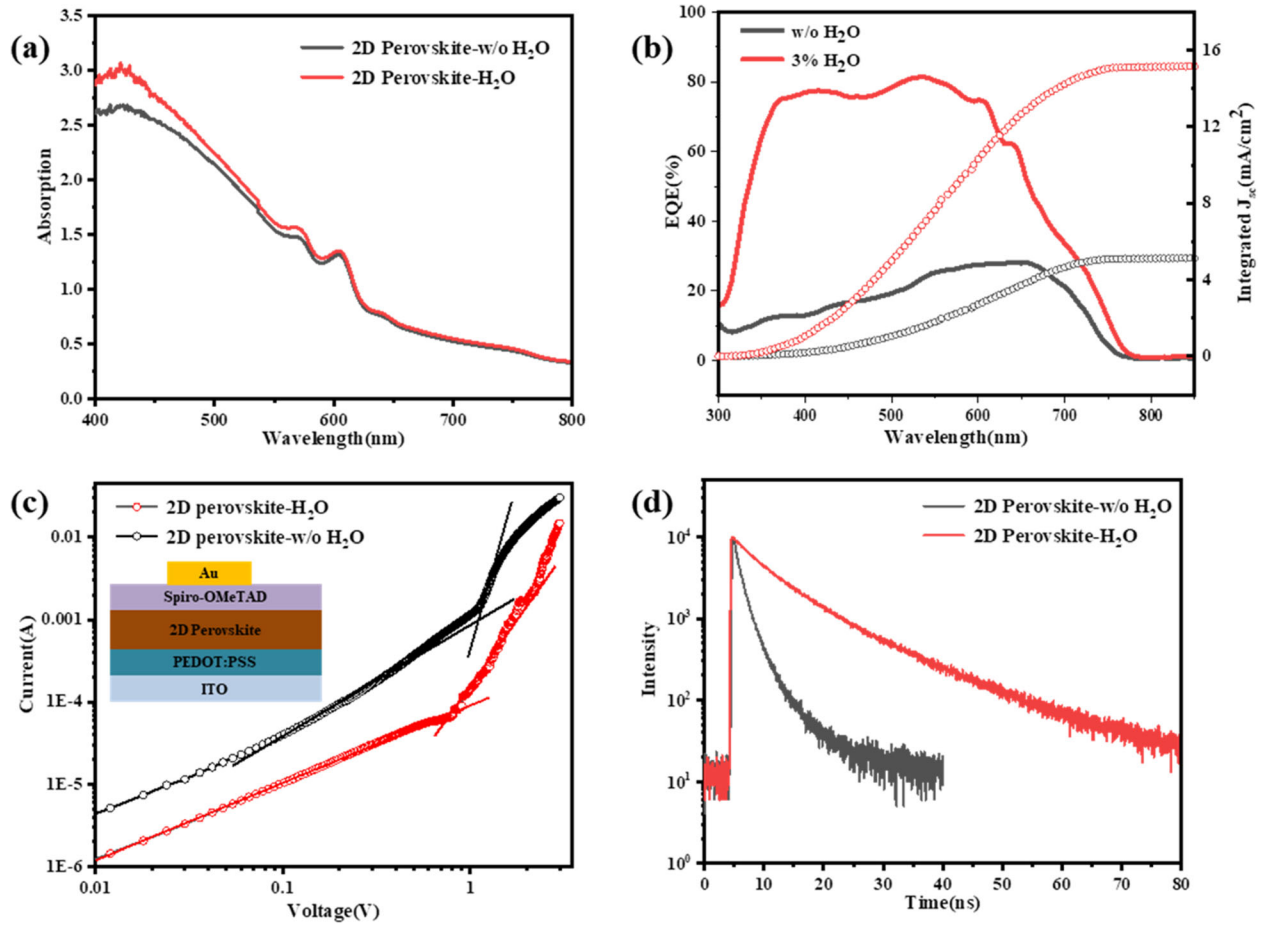

Fig. 4 **a** Absorption spectra of $BA_2MA_3Pb_4I_{13}$ films without and with 3% H_2O. **b** EQE spectra and integrated current curve of corresponding devices. **c** Dark current-voltage curves of the HODs based on corresponding 2D perovskite films (inset: configuration of HODs). **d** TRPL spectra of corresponding 2D perovskite films

perovskite-3% H_2O film shows a slightly enhanced absorption in the range of 400-600 nm compared with the perovskite-w/o H_2O film. From the cross-section SEM images (insets of Fig. 3a-c), it can be concluded that all 2D perovskite films show almost the same thickness. Thus, we attribute the enhanced absorption to a uniform, highly crystalline, and highly oriented perovskite film induced by water additive [14, 48]. The external quantum efficiency (*EQE*) spectrums of PVSC without H_2O additive and PVSC with 3% H_2O are shown in Fig. 4b, and the corresponding derived integrated current values are plotted on the right *y*-axis. The integrated J_{sc} from *EQE* spectrum of PVSC without H_2O additive and the PVSC with 3%H_2O is 5.16 mA/cm^2 and 15.20 mA/cm^2, respectively. The values are close to the results measured from J–V curve. Apparently, the EQE values of the device with 3% H_2O in most visible light range are much higher than that of the device without additive. This phenomenon not only results from enhanced light absorption but also mainly comes from more efficient charge transport in highly oriented 2D perovskite film with better crystallinity.

Further, we measured the dark current-voltage curves of the hole-only devices (HODs) with a structure of ITO/PEDOT:PSS/2D perovskite/Spiro-OMeTAD/Au to characterize the trap-state density (N_t) in 2D perovskite films (Fig. 4v). The N_t was determined by the trap-filled limit voltage (V_{TFL}) according to equation (1) [14, 46, 49]:

$$N_t = \frac{2\varepsilon_0\varepsilon_r V_{TFL}}{qL^2} \quad (1)$$

where ε_o is the vacuum permittivity, ε_r is the relative dielectric constant of 2D perovskite, q is the elemental charge, and L is the thickness of the 2D perovskite film. Both perovskite films have the same ε_r value and the same thickness. Therefore, the N_t is positively correlated with the V_{TFL} value. As shown in Fig. 4c, the V_{TFL} value obtained from 2D perovskite-3% H_2O based HOD is obviously lower than that obtained from 2D perovskite-w/

o H_2O based HOD. It demonstrates that trap-state density in the 2D perovskite-3% H_2O film has been reduced. This was further confirmed by the time-resolved photoluminescence (TRPL) spectra of the 2D perovskite films deposited on nonconductive glass. The time decay of the fluorescence signals was fitted to two exponentials, as depicted in Fig. 4d. Benefited from high-quality films with few grain boundaries as evidenced in Fig. 2, the 2D perovskite-3% H_2O film has a longer fluorescence lifetime of 10 ns compared with 2D perovskite-w/o H_2O film (2 ns), demonstrating the reduced bulk defect density in 2D perovskite-3% H_2O film.

Based on all above results, we prove that incorporating suitable water additive in precursor solution can control the crystal growth of $BA_2MA_3Pb_4I_{13}$ perovskite film with enlarged grain size and uniform film coverage, leading to a reduced trap-state density. And this highly crystalline and highly oriented $BA_2MA_3Pb_4I_{13}$ perovskite films induced by water additive would facilitate charge transport [8, 9, 14]. Therefore, the high-quality $BA_2MA_3Pb_4I_{13}$ perovskite films bring a comprehensive improvement in V_{oc}, J_{sc}, FF of the corresponding PVSCs.

Conclusion

In conclusion, we have investigated the effects of H_2O additive on 2D $BA_2MA_3Pb_4I_{13}$ perovskite thin films and the corresponding device performance. By optimizing the amount of H_2O additive, surface morphology, grain size, and crystallinity of the $BA_2MA_3Pb_4I_{13}$ film are obviously improved and preferred crystalline orientation was obtained. Therefore, optimized 3% H_2O additive based 2D PVSC yields a significant improvement in PCE from 2.29 to 12.15%. Meanwhile, the shelf stability of the devices is also improved. Our results prove that controlling 2D perovskite crystallization via H_2O additive is an effective way to obtain efficient and stable 2D PVSCs.

Abbreviations

2D: Two-dimensional; PCE: Power conversion efficiency; PVSCs: Perovskite solar cells; PEA^+: Phenethylammonium; BA^+: Butyl ammonium; H_2O: Water; NH_4SCN: Ammonium thiocyanate; NH_4Cl: Ammonium chloride; DMSO: Dimethyl sulfoxide; TSC: Thiosemicarbazide; MAI: Methyl-ammonium iodide; BAI: n-butylammonium iodide; $PC_{61}BM$: Phenyl-C61-butyric acid methyl ester; BCP: Bathocuproine; spiro-MeOTAD: 2,29,7,79-tetrakis(N,N-di-p-methoxyphenylamine)-9,9-spirobifluorene); ITO: Indium tin oxide; *J-V*: Current density-voltage; SEM: Scanning electron microscope; GIWAXS: Grazing incidence wide-angle X-ray scatting; *EQE*: External quantum efficiencies; TRPL: Time-resolved photoluminescence; V_{oc}: Circuit voltage; J_{sc}: Short-circuit current density; *FF*: Fill factor; HODs: Hole-only devices

Acknowledgements

The authors greatly acknowledge the Chongqing Engineering Research Center of New Energy Storage Devices and Applications and Ceshigou Analytical Testing Company for the measurement assistance.

Authors' Contributions

ZL and HZ wrote the article and carried out the experiment together. DL revised the article. ZL and WY gave equipment support. HC, LJ, SY, and YG performed the SEM, GIWAXS, UV-Vis absorption, and TRPL data analysis, respectively. SL supervised the whole project and interpreted the results. The authors read and approved the final manuscript.

Funding

This work was supported by the National Natural Science Foundation of China under Grant Nos. 61874150, 61421002, and 61574029. This work was also partially supported by the Natural Science Foundation of Chongqing (cstc2019jcyj-msxmX0824).

Availability of Data and Materials

All the data are fully available without restrictions.

Competing Interests

The authors declare that they have no competing interests.

Author details

[1]State Key Laboratory of Electronic Thin Films and Integrated Devices, and School of Optoelectronic Science and Engineering, University of Electronic Science and Technology of China (UESTC), Chengdu 610054, Sichuan, China. [2]Chongqing Engineering Research Center of New Energy Storage Devices and Applications, Chongqing University of Arts and Sciences, Chongqing 402160, People's Republic of China.

Received: 19 March 2020 Accepted: 28 April 2020
Published online: 13 May 2020

References

1. Grancini G, Nazeeruddin MK (2018) Dimensional tailoring of hybrid perovskites for photovoltaics. Nat. Rev. Mater. 4:4–22
2. Wang P, Wu Y, Cai B, Ma Q, Zheng X, Zhang WH (2019) Solution-processable perovskite solar cells toward commercialization: progress and challenges. Adv. Funct. Mater. 29:1807661
3. Zhang L, Liu Y, Yang Z, Liu S (2019) Two dimensional metal halide perovskites: promising candidates for light-emitting diodes. J. Energy Chem. 37:97–110
4. Hong, X.;Ishihara, T.; Nurmikko, A. V. Dielectric confinement effect on excitons in PbI4-based layered semiconductors. Physical review. B, Condens. Matter 1992, 45, 6961-6964.
5. Sum TC, Mathews N (2014) Advancements in perovskite solar cells: photophysics behind the photovoltaics. Energ. Environ. Sci. 7:2518–2534
6. NREL: National Center For Photovoltaics Home Page. [Online]. https://www.nrel.gov/pv/assets/pdfs/best-research-cell-efficiencies-190416.pdf. Accessed 16 February 2020.
7. Tsai, H. H.;Nie, W. Y.;Blancon, J. C.;Toumpos, C. C. S.;Asadpour, R.;Harutyunyan, B.;Neukirch, A. J.;Verduzco, R.;Crochet, J. J.;Tretiak, S.;Pedesseau, L.;Even, J.; Alam, M. A.;Gupta, G.;Lou, J.;Ajayan, P. M.;Bedzyk, M. J.;Kanatzidis, M. G.; Mohite, A. D. High-efficiency two-dimensional Ruddlesden-Popper perovskite solar cells. Nature 2016, 536, 312–+.
8. Zhang X, Wu G, Yang S, Fu W, Zhang Z, Chen C, Liu W, Yan J, Yang W, Chen H (2017) Vertically oriented 2D layered perovskite solar cells with enhanced efficiency and good stability. Small 13
9. Zhang XQ, Wu G, Fu WF, Qin MC, Yang WT, Yan JL, Zhang ZQ, Lu XH, Chen HZ (2018) Orientation regulation of phenylethylammonium cation based 2D perovskite solar cell with efficiency higher than 11%. Adv. Energy Mater. 8
10. Qing J, Liu X-K, Li M, Liu F, Yuan Z, Tiukalova E, Yan Z, Duchamp M, Chen S, Wang Y, Bai S, Liu J-M, Snaith HJ, Lee C-S, Sum TC, Gao F (2018) Aligned and graded type-II Ruddlesden-Popper perovskite films for efficient solar cells. Adv. Energy Mater. 8:1800185
11. Yu S, Yan Y, Chen Y, Chábera P, Zheng K, Liang Z (2019) Enabling room-temperature processed highly efficient and stable 2D Ruddlesden–Popper perovskite solar cells with eliminated hysteresis by synergistic exploitation of additives and solvents. J. Mater. Chem. A 7:2015–2021
12. Fu W, Wang J, Zuo L, Gao K, Liu F, Ginger D (2018) S.; Jen, A. K. Y. Two-dimensional perovskite solar cells with 14.1% power conversion efficiency and 0.68% external radiative efficiency. ACS Energy Lett. 3:2086–2093
13. Lian X, Chen J, Fu R, Lau T-K, Zhang Y, Wu G, Lu X, Fang Y, Yang D, Chen H (2018) An inverted planar solar cell with 13% efficiency and a sensitive visible light detector based on orientation regulated 2D perovskites. J. Mater. Chem. A 6:24633–24640

14. Zheng H, Liu D, Wang Y, Yang Y, Li H, Zhang T, Chen H, Ji L, Chen Z, Li S (2020) Synergistic effect of additives on 2D perovskite film towards efficient and stable solar cell. Chem. Eng. J. 389:124266
15. Chen YN, Sun Y, Peng JJ, Zhang W, Su XJ, Zheng KB, Pullerits T, Liang ZQ (2017) Tailoring organic cation of 2D air-stable organometal halide perovskites for highly efficient planar solar cells. Adv. Energy Mater. 7
16. Zhang X, Ren X, Liu B, Munir R, Zhu X, Yang D, Li J, Liu Y, Smilgies D-M, Li R, Yang Z, Niu T, Wang X, Amassian A, Zhao K, Liu S (2017) Stable high efficiency two-dimensional perovskite solar cells via cesium doping. Energ. Environ. Sci. 10:2095–2102
17. Zhou N, Shen Y, Li L, Tan S, Liu N, Zheng G, Chen Q, Zhou H (2018) Exploration of crystallization kinetics in quasi two-dimensional perovskite and high performance solar cells. J. Am. Chem. Soc. 140:459–465
18. Proppe AH, Quintero-Bermudez R, Tan H, Voznyy O, Kelley SO, Sargent EH (2018) Synthetic control over quantum well width distribution and carrier migration in low-dimensional perovskite photovoltaics. J. Am. Chem. Soc. 140:2890–2896
19. Tan, S.;Zhou, N.;Chen, Y.;Li, L.;Liu, G.;Liu, P.;Zhu, C.;Lu, J.;Sun, W.;Chen, Q.; Zhou, H. Effect of high dipole moment cation on layered 2D organic–inorganic halide perovskite solar cells. Adv. Energy Mater. 2018, 10.1002/aenm.201803024, 1803024.
20. Lian X, Chen J, Qin M, Zhang Y, Tian S, Lu X, Wu G, Chen H (2019) The second spacer cation assisted growth of a 2D perovskite film with oriented large grain for highly efficient and stable solar cells. Angew. Chem. 58:9409–9413
21. Chen S, Shen N, Zhang L, Kong W, Zhang L, Cheng C, Xu B (2019) Binary organic spacer-based quasi-two-dimensional perovskites with preferable vertical orientation and efficient charge transport for high-performance planar solar cells. J. Mater. Chem. A 7:9542–9549
22. Gao L, Zhang F, Chen X, Xiao C, Larson BW, Dunfield SP, Berry JJ, Zhu K (2019) Enhanced charge transport by incorporating formamidinium and cesium cations into two-dimensional perovskite solar cells. Angew. Chem. 58:11737–11741
23. Zhou N, Huang B, Sun M, Zhang Y, Li L, Lun Y, Wang X, Hong J, Chen Q, Zhou H (2019) The spacer cations interplay for efficient and stable layered 2D perovskite solar cells. Adv. Energy Mater. 10:1901566
24. Ren H, Yu S, Chao L, Xia Y, Sun Y, Zuo S, Li F, Niu T, Yang Y, Ju H, Li B, Du H, Gao X, Zhang J, Wang J, Zhang L, Chen Y, Huang W (2020) Efficient and stable Ruddlesden–Popper perovskite solar cell with tailored interlayer molecular interaction. Nat. Photonics 14:154–163
25. Jiang Y, He X, Liu T, Zhao N, Qin M, Liu J, Jiang F, Qin F, Sun L, Lu X, Jin S, Xiao Z, Kamiya T, Zhou Y (2019) Intralayer A-site compositional engineering of Ruddlesden–Popper perovskites for thermostable and efficient solar cells. ACS Energy Lett. 4:1216–1224
26. Ma C, Shen D, Ng T-W, Lo M-F, Lee C-S (2018) 2D Perovskites with short interlayer distance for high-performance solar cell application. Adv. Mater. 30:1800710
27. Qiu J, Zheng Y, Xia Y, Chao L, Chen Y, Huang W (2018) Rapid crystallization for efficient 2D Ruddlesden–Popper (2DRP) perovskite solar cells. Adv. Funct. Mater. 29:1806831
28. Gao L, Zhang F, Xiao C, Chen X, Larson BW, Berry JJ, Zhu K (2019) Improving charge transport via intermediate-controlled crystal growth in 2D perovskite solar cells. Adv. Funct. Mater. 29:1901652
29. Zhang JJ, Zhang LY, Li XH, Zhu XY, Yu JG, Fan K (2019) Binary solvent engineering for high-performance two-dimensional perovskite solar cells. ACS Sustain. Chem. Eng. 7:3487–3495
30. Mao P, Zhuang J, Wei Y, Chen N, Luan Y, Wang J (2019) Origin and suppression of the graded phase distribution in Ruddlesden-Popper perovskite films for photovoltaic application. Solar RRL 3:1800357
31. Chen J, Lian X, Zhang Y, Yang W, Li J, Qin M, Lu X, Wu G, Chen H (2018) Interfacial engineering enables high efficiency with a high open-circuit voltage above 1.23 V in 2D perovskite solar cells. J. Mater. Chem. A 6:18010–18017
32. Liu T, Jiang Y, Qin M, Liu J, Sun L, Qin F, Hu L, Xiong S, Jiang X, Jiang F, Peng P, Jin S, Lu X, Zhou Y (2019) Tailoring vertical phase distribution of quasi-two-dimensional perovskite films via surface modification of hole-transporting layer. Nat. Commun. 10:878
33. Lian XM, Chen JH, Zhang YZ, Tian SX, Qin MC, Li J, Andersen TR, Wu G, Lu XH, Chen HZ (2019) Two-dimensional inverted planar perovskite solar cells with efficiency over 15% via solvent and interface engineering. J. Mater. Chem. A 7:18980–18986
34. Zhang Y, Wang P, Tang MC, Barrit D, Ke W, Liu J, Luo T, Liu Y, Niu T, Smilgies DM, Yang Z, Liu Z, Jin S, Kanatzidis MG, Amassian A, Liu SF, Zhao K (2019) Dynamical transformation of two-dimensional perovskites with alternating cations in the interlayer space for high-performance photovoltaics. J. Am. Chem. Soc. 141:2684–2694
35. Wu G, Zhou J, Zhang J, Meng R, Wang B, Xue B, Leng X, Zhang D, Zhang X, Bi S, Zhou Q, Wei Z, Zhou H, Zhang Y (2019) Management of the crystallization in two-dimensional perovskite solar cells with enhanced efficiency within a wide temperature range and high stability. Nano Energy 58:706–714
36. Zhang J, Qin J, Wang M, Bai Y, Zou H, Keum JK, Tao R, Xu H, Yu H, Haacke S, Hu B (2019) Uniform permutation of quasi-2D perovskites by vacuum poling for efficient, high-fill-factor solar cells. Joule 3:3061–3071
37. Wu G, Li X, Zhou J, Zhang J, Zhang X, Leng X, Wang P, Chen M, Zhang D, Zhao K, Liu SF, Zhou H, Zhang Y (2019) Fine multi-phase alignments in 2D perovskite solar cells with efficiency over 17% via slow post-annealing. Adv. Mater. 31:e1903889
38. Zhang F, Bi DQ, Pellet N, Xiao CX, Li Z, Berry JJ, Zakeeruddin SM, Zhu K, Gratzel M (2018) Suppressing defects through the synergistic effect of a Lewis base and a Lewis acid for highly efficient and stable perovskite solar cells. Energ. Environ. Sci. 11:3480–3490
39. He T, Liu Z, Zhou Y, Ma H (2018) The stable perovskite solar cell prepared by rapidly annealing perovskite film with water additive in ambient air. Sol. Energy Mater. Sol. Cells 176:280–287
40. Gong X, Li M, Shi XB, Ma H, Wang ZK, Liao LS (2015) Controllable perovskite crystallization by water additive for high-performance solar cells. Adv. Funct. Mater. 25:6671–6678
41. Zhang W, Xiong J, Li J, Daoud WA (2019) Mechanism of water effect on enhancing the photovoltaic performance of triple-cation hybrid perovskite solar cells. ACS Appl. Mater. Interfaces 11:12699–12708
42. Solanki A, Lim SS, Mhaisalkar S, Sum TC (2019) Role of water in suppressing recombination pathways in CH3NH3PbI3 perovskite solar cells. ACS Appl. Mater. Interfaces 11:25474–25482
43. Wu C-G, Chiang C-H, Tseng Z-L, Nazeeruddin MK, Hagfeldt A, Grätzel M (2015) High efficiency stable inverted perovskite solar cells without current hysteresis. Energ. Environ. Sci. 8:2725–2733
44. Adhikari N, Dubey A, Gaml EA, Vaagensmith B, Reza KM, Mabrouk SA, Gu S, Zai J, Qian X, Qiao Q (2016) Crystallization of a perovskite film for higher performance solar cells by controlling water concentration in methyl ammonium iodide precursor solution. Nanoscale 8:2693–2703
45. Xin D, Tie S, Yuan R, Zheng X, Zhu J, Zhang WH (2019) Defect passivation in hybrid perovskite solar cells by tailoring the electron density distribution in passivation molecules. ACS Appl. Mater. Interfaces 11:44233–44240
46. Liu Z, Liu D, Chen H, Ji L, Zheng H, Gu Y, Wang F, Chen Z, Li S (2019) Enhanced crystallinity of triple-cation perovskite film via doping NH4SCN. Nanoscale Res. Lett. 14:304
47. Heo, J. H.;Song, D. H.; Im, S. H. Planar CH3NH3PbBr3 hybrid solar cells with 10.4% power conversion efficiency, fabricated by controlled crystallization in the spin-coating process. Adv. Mater. 2014, 26, 8179-8183.
48. Feng M, You S, Cheng N, Du J (2019) High quality perovskite film solar cell using methanol as additive with 19.5% power conversion efficiency. Electrochim. Acta 293:356–363
49. Chen Y, Yang Z, Wang S, Zheng X, Wu Y, Yuan N, Zhang WH, Liu SF (2018) Design of an inorganic mesoporous hole-transporting layer for highly efficient and stable inverted perovskite solar cells. Adv. Mater. 30:e1805660

Publisher's Note